Applied Energy 316 (2022) 119115

Contents lists available at ScienceDirect

Applied Energy

journal homepage: www.elsevier.com/locate/apenergy

Catalytic hydropyrolysis of lignin using NiMo-doped catalysts: Catalyst evaluation and mechanism analysis

Tan Li, Jing Su, Huiyuan Wang, Cong Wang, Wen Xie, Kaige Wang *

State Key Laboratory of Clean Energy Utilization, Zhejiang University, Hangzhou 310027, China

HIGHLIGHTS

- A NiMo-doped catalyst with optimal Ni/Mo ratio and carrier led to hydrocarbon bio-oil with low selectivity of poly-aromatics and methane.
- Two coefficients were proposed to qualitatively evaluate the activity of NiMo catalysts.
- The effect of hydrogen pressure on catalytic activity of NiMo-doped catalysts was illustrated.
- The synergistic mechanism of Ni and Mo was studied during the catalytic hydropyrolysis of lignin.
- The evolution mechanism of lignin hydropyrolysis volatiles over NiMo/ZrO_2 was proposed.

GRAPHICAL ABSTRACT

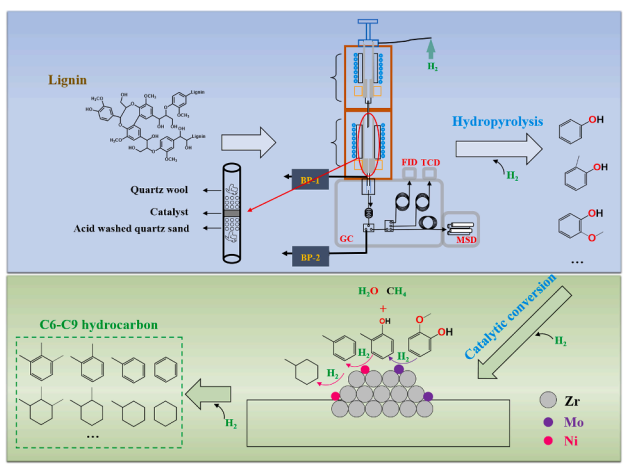

ARTICLE INFO

Keywords:
Hydropyrolysis
Lignin
Pyrolysis mechanism
NiMo-doped catalyst

ABSTRACT

NiMo-doped catalysts were investigated for the conversion of lignin to drop-in fuel through catalytic hydropyrolysis. The influence of NiMo-doped catalysts with different carriers and Ni/Mo molar ratios on the hydropyrolysis product distribution were studied using both lignin and lignin model compounds. Two coefficients were proposed to qualitatively evaluate the catalytic performance of NiMo-doped catalysts. Low yield of methane (13.04c%) and high yield of condensable hydrocarbons products (25.82c%) with low selectivity of polyaromatics (4.37%) were obtained at 1.0 MPa H_2 and 400 °C catalytic temperature during lignin catalytic hydropyrolysis over Ni_1Mo/ZrO_2. The hydrodeoxygenation activity of Ni_xMo/ZrO_2 depends on Ni^0, Mo^{4+}, and Mo^{3+}. The synergistic effect of Ni and Mo promotes the removal of the phenolic methoxy group. The increase in hydrogen pressure tends to make hydrogen to be consumed through hydrocracking and hydrogenation reactions. The influence of Ni_1Mo/ZrO_2 on evolution of lignin hydropyrolysis volatiles was revealed. Ni shows strong activity in

Abbreviations: NH_3-TPD, Temperature-programmed desorption of ammonia; XRD, X-ray diffraction; XPS, X-ray photoelectron spectroscopy; GC, Gas Chromatograph; MS, Mass Spectrometer; FID, Flame Ionization Detector; TCD, Thermal Conductivity Detector; CHC, Saturated cycloalkanes; MAH, Monocyclic aromatic hydrocarbon; PAH, Polycyclic aromatic hydrocarbons; CCH, Condensable chain hydrocarbons with carbon number greater than 4; GHC, Gaseous hydrocarbon products.

* Corresponding author.
E-mail address: kaigewang@zju.edu.cn (K. Wang).

https://doi.org/10.1016/j.apenergy.2022.119115
Received 8 February 2022; Received in revised form 22 March 2022; Accepted 8 April 2022
Available online 14 April 2022

the removal of phenolic hydroxyl groups and benzene ring hydrogenation, while Mo tends to remove phenolic methoxy groups.

1. Introduction

The use of renewable lignocellulosic biomass to produce sustainable drop-in biofuel through fast pyrolysis has been studied for many years [1–3]. Among the major components of biomass, lignin with phenylpropyl structure is the most difficult one to be utilized. Lignin pyrolysis produces a mixture of oxygenates with high oxygen content, which prevents it from being used directly as transportation fuel or high-value chemicals [4]. Recently, catalytic pyrolysis using zeolite catalysts and metal oxide catalysts under hydrogen atmosphere has been developed to process lignin or whole biomass for production of high-quality bio-crude [5,6].

Although the zeolite catalysts have been extensively explored in biomass conversion, the excessive coke formation and high selectivity for polyaromatics have hindered its development [7,8]. The limited hydrogenation or deoxygenation capacity of metal oxide catalysts (such as MoO_3, TiO_2, Al_2O_3, ZrO_2), which leads to high oxygen content and low heating value in bio-oil, also hinders their applications in biomass hydropyrolysis process [9–11]. Therefore, it is necessary to explore hydrodeoxygenation catalysts suitable for hydrogen atmosphere.

NiMo-doped catalysts have been widely used in the conversion of bio- or petroleum-based feedstocks due to their excellent hydrodeoxygenation capacity. Shi et al. [12] carried out catalytic hydropyrolysis experiments of pine using NiMo-doped HZSM-5 catalyst on a two-stage fixed bed reactor. The highest hydrocarbon bio-oil yield was 23.9 wt%. The appropriate ratio of Ni and Mo on HZSM-5 improves the synergistic effect of Ni and Mo to achieve high condensable hydrocarbon yield. Yu et al. [13] used sulfided NiMo/γ-Al_2O_3 catalysts on a fixed bed to carry out catalytic hydropyrolysis experiments of bio-oil model compounds. The conversion rates of phenol and 1-methyl naphthalene were 100% and 89.4%, respectively. The appropriate pore size (10–20 nm) of sulfided NiMo/γ-Al_2O_3 is thought to be responsible for the excellent hydrodeoxygenation effect. Dayton et al. [14] used a commercial NiMo-doped catalyst in a fluidized bed to conduct pine catalytic hydropyrolysis experiments. 23.7 wt% bio-crude with less than 1 wt% oxygen content and 29.7% selectivity of polyaromatics was obtained. They also reported that the increase in hydrogen concentration can suppress the formation of oxygenates and polyaromatics by enhancing the hydrogenation and hydrocracking reactions. Stummann et al. [15] used three doped metal oxide catalysts on a fluidized bed reactor to carry out bark-free beech wood catalytic hydropyrolysis experiments. 24.3 wt% bio-crude with 13% selectivity of polyaromatics was obtained which is due to the high hydrogenation activity and cracking activity of NiMo/$MgAl_2O_4$. It should be emphasized that polymeric aromatics as carbon precursors are not ideal components to enhance the calorific value of high-quality bio-oils. Therefore, strictly controlling the content of polycyclic aromatics is very important to improve the quality of bio-oil. Sun et al. [16] inferred that –OH group, $–CH_3$ group, and benzene radicals promote the formation of polyaromatics such as naphthalene and biphenyl. To the best of our knowledge, the Mo loading in NiMo-doped catalysts can be adjusted to promote the removal of –OH groups in the form of water [17], which will unbalance the reaction to generate polymeric aromatic hydrocarbons.

In addition to the high selectivity for polyaromatics in the pyrolysis products, an increase in methane yield at the expense of bio-oil yield was also reported after applying the NiMo-doped catalysts in biomass hydropyrolysis. Wang et al. [18] conducted catalytic hydropyrolysis experiments under atmosphere pressure with three types of woody biomass on a fluidized bed reactor. High activity of a commercial NiMo doped catalyst led to high methane yields of over 50% at 863 K. Yu et al. [19] carried out catalytic hydropyrolysis experiments of miscanthus × giganteus using Ni-ZSM-5/Ni-MCM-41 catalyst on a Py-GC/MS system and reported a methane yield of about 45 mol%, which is due to the fact that hydrogen promotes the methanation reaction on the Ni site. Resende et al. [20] conducted biomass catalytic hydropyrolysis experiments in a fluidized bed reactor. The results reported that the introduction of 2.7 wt% Mo onto 1.4 wt% Ni/HZSM-5 could drastically decrease the methane yield from 22.6c% to 9.3c%. They speculated that methane oligomerizes on the molybdenum site to form aromatic hydrocarbons, which are then hydrogenated to form larger alkanes. In order to reduce the formation of methane, the methanation reaction should be suppressed by adjusting the Ni loading or optimizing the synergistic effect of Ni and Mo in NiMo-doped catalysts [21,22]. Although NiMo-doped catalysts have been extensively used in biomass conversion, the detailed hydrodeoxygenation mechanism of biomass catalytic hydropyrolysis volatiles and the synergistic effect of Ni and Mo still need to be explored more comprehensively.

The purpose of this work is to clarify the synergistic mechanism of NiMo-doped catalysts and select a NiMo-doped catalyst with high condensable hydrocarbon yield and low selectivity to polyaromatics and methane. NiMo-doped catalysts with different carriers and Ni/Mo molar ratios were prepared by the wetness impregnation method. The ex-situ catalytic hydropyrolysis experiments of lignin and its model compounds were carried out in a furnace-type micro-reactor with the highest operating pressure of 3.5 MPa. Two dimensionless coefficients were proposed to compare the hydrogenation activity, hydrodeoxygenation activity and hydrocracking activity of different NiMo-doped catalysts. The results from catalytic hydropyrolysis experiments of lignin model compounds over NiMo-doped ZrO_2 with different Ni/Mo molar ratios revealed the hydrodeoxygenation mechanism of lignin hydropyrolysis volatiles.

2. Experimental section

2.1. Materials

Milled wood lignin extracted from Chinese fir was used as the feedstock for the hydropyrolysis experiments. The preparation method of milled wood lignin was described in previous studies [23,24]. Ultimate analysis was carried out in an organic elemental analyzer (Vario micro cube, Elementar). The C, H, O, N content of the lignin was 62.32%, 6.24%, 31.33%, and 0.11%, respectively. Phenol, o-methoxy- (AR, 99%, D & B), phenol, 3-methyl- (AR, 99%, Macklin), and toluene (AR, 99%, Macklin) were used as lignin model compounds to verify the catalytic hydropyrolysis mechanism.

Mo/ZrO_2, Ni_1Mo/Fe_2O_3, Ni_1Mo/γ-Al_2O_3, Ni_1Mo/TiO_2, and Ni_xMo/ZrO_2 catalysts (x represents the Ni/Mo atomic ratio) were prepared by the wetness impregnation method. The nominal Mo mass content in these catalysts is set to 10 wt% of the carriers. Ammonium molybdate tetrahydrate ($(NH_4)_6Mo_7O_{24}\cdot 4H_2O$) and nickel nitrate hexahydrate ($Ni(NO_3)_2\cdot 6H_2O$), nano zirconia (ZrO_2), nano titanium oxide (TiO_2), iron oxide (Fe_2O_3) and alumina (γ-Al_2O_3) were purchased from Aladdin. Before impregnation, ZrO_2, γ-Al_2O_3, Fe_2O_3 and TiO_2 were calcined in a muffle furnace at 550 °C for 4 h, respectively. A calculated amount of metal precursor was dissolved in deionized water. The mixed solution was added to the calculated amount of metal oxide to form a slurry. The slurry was heated to 80 °C and stirred for 3 h. The suspension was then cooled to room temperature and dried at 110 °C overnight. The dried catalyst was calcined at 550 °C for 4 h and then reduced at 550 °C for 4 h in the hydrogen with a flow rate of 80 mL/ min. All catalysts were pelletized, crushed and then sieved into 40–60 mesh.

2.2. Catalyst characterization

The surface area and porosity of the catalysts were measured by N_2 temperature-programmed-desorption on a Micromeritics ASAP 2460 instrument. Before the measurement, the samples were outgassed under vacuum at 200 °C for 8 h.

Temperature-programmed desorption of ammonia (NH_3-TPD) was conducted in a Bel Cata II Chemisorption analyzer for the characterization and quantification of catalyst's acid sites. The samples were first heated to 300 °C at 10 °C/min in 30 mL/min He and held for 1 h to remove moisture. Then, the temperature was lowered to 50 °C and NH_3 was adsorbed for 1 h by flowing 10 vol% NH_3/He at 30 mL/min. After that, purged with He (30 mL/min) for 1 h, the samples were heated to 850 °C at 10 °C/min. The NH_3 desorption was recorded using a thermal conductivity detector (TCD).

The X-ray diffraction (XRD) patterns were collected in a 2-theta range of 5°-90° at a scanning rate of 5°/min on the X-ray powder diffractometer (Smartlab 9kw, Rigaku) using Cu Kα (λ = 1.5406 Å) irradiation.

The oxidation state of the metal on the sample's surface was determined by X-ray photoelectron spectroscopy (XPS) in a Thermo Scientific K-Alpha with Al Kα monochromatic radiation (hν, 1486.6 eV). The C1s peak was set to 284.80 eV to internally calibrate the energy scale.

2.3. Catalyst testing

Performance tests of the catalysts were conducted in a tandem microreactor system (Rx-3050 TR, Frontier Laboratories, Japan) equipped with a high-pressure module. A schematic diagram of the system was shown in **Fig. S.1**. Approximately 0.5 mg lignin was pyrolyzed in the 1st reactor. The pyrolysis vapor was purged to the 2nd reactor by H_2 with a flow rate of 56 mL/min. A quartz tube loaded with 4 mg catalyst was placed in the 2nd reactor. The temperature of the 1st and 2nd interface was kept at 300 °C to prevent product condensation. For the verification experiments using lignin model compounds, the liquid model compound (1 μL) was directly injected into the 1st reactor through the liquid sampler for the micro-pyrolyzer by a liquid syringe. Before injecting the liquid model compound, the liquid syringe was rinsed three times with the sample to be tested. After injecting the liquid model compound, the syringe was rinsed three times with acetone. The pyrolysis products were analyzed on-line by a gas chromatograph (GC) (7890B, Agilent Technologies, USA) equipped with a flame ion detector (FID), TCD, and mass spectrometer (MS) (5977B, Agilent Technologies, USA). The GC oven was programmed for an 8 min held at 30 °C then ramped at 5 °C/min to 250 °C, after which temperature was held constant for 4 min.

The condensable and non-condensable products were quantified with external standards. The mass of char formed in the pyrolysis stage was determined by weighing the mass of the sample cup before and after the reaction by using a microbalance (XPR10, Mettler Toledo, Switzerland). To ensure experimental repeatability, all experiments were performed in triplicate. In this paper, condensable hydrocarbons are defined as hydrocarbons with a carbon number greater than 4, including aromatic hydrocarbons, chain alkanes, and cyclic alkanes. Condensable chain hydrocarbons are defined as chain alkanes with carbon number greater than 4.

The carbon yield, the selectivity of products, the conversion rate of the lignin model compound, *HCH*, and *HCHD* were calculated by the equations below, respectively:

$$Carbonyieldofproduct = \frac{Thecarbonmassinproducts}{Thetotalcarbonmassinfeedstock} \times 100\% \quad (1)$$

$$Selectivity = \frac{Thetotalcarbonmassinspecificliquid/gasproducts}{Thetotalcarbonmassinliquid/gasproducts} \times 100\% \quad (2)$$

$$Conversion = (1 - theremainingamountoffeedstock) \times 100\% \quad (3)$$

$$HCH = \frac{Thetotalcarbonyieldinchainhydrocarbonproducts}{Thetotalcarbonyieldincycloalkaneproducts} \quad (4)$$

The ratio of hydrocracking reaction activity to hydrogenation reaction activity is abbreviated as *HCH*. The chain hydrocarbon products include gaseous hydrocarbons and condensable chain hydrocarbons. It is reported that gaseous hydrocarbons and condensable chain hydrocarbons are produced from pyrolysis vapor by a cracking reaction [25,26]. The saturation of the benzene ring structure is attributed to the enhanced hydrogenation reaction activity under the action of the catalyst. Therefore, it is reasonable to use the total yields of gaseous hydrocarbons and condensable chain hydrocarbons stand for the hydrocracking reaction activity and the total yield of cycloalkane products stands for hydrogenation reaction activity. In order to prove that the phenolics in the pyrolysis products have nothing to do with the cracking ability of the catalyst, a milled wood lignin hydropyrolysis experiment (1.0 MPa H_2, pyrolysis temperature: 500 °C, catalytic temperature: 400 °C) was carried out. Relevant discussion is added to the supplementary file.

$$HCHD = \frac{Thetotalcarbonyieldinchainhydrocarbonproducts}{Thetotalcarbonyieldincondensablehydrocarbonproducts} \quad (5)$$

The ratio of hydrocracking reaction activity to hydrodeoxygenation reaction activity is abbreviated as *HCHD*. It is reported that the hydrodeoxygenation reaction that occurred in lignin pyrolysis vapor produces condensable hydrocarbons [27–29]. This is also verified in catalytic hydropyrolysis experiments with lignin model compounds. Therefore, it is reasonable to use the total yield of condensable hydrocarbon products stands for the hydrodeoxygenation reaction activity.

3. Results and discussion

3.1. Characterization of catalysts

The basic information of the catalysts used in the hydropyrolysis experiments is shown in Table 1.

The types of carriers have obvious effects on the physical parameters of the catalysts. Ni_1Mo/Al_2O_3 showed the largest BET specific surface area, the largest proportion of mesopores, and the smallest mesopore size (8.23 nm). Yu et al. reported that pores with a pore diameter of 5–10 nm contribute to the hydrogenation conversion of most aromatics [13]. Compared with the ZrO_2, the surface area and total pore volume of Mo/ZrO_2 slightly decreased after loading Mo. The surface and pores of ZrO_2 were blocked by loading Mo [30]. In addition, the BET specific surface area, total pore volume, and mesopores proportion of Mo/ZrO_2 increased when Ni was introduced. This is because the interaction between Ni and ZrO_2 is weak, which inhibits the diffusion of Ni into the pores of ZrO_2 and promotes the formation of mesopores [31].

The XRD pattern of each catalyst is shown in Fig. 1. For ZrO_2, the sharp peaks positioned at 2θ = 28.2°, 31.4°, and 34.1° were attributed to m-ZrO_2. A diffraction peak (37.0°) of bulk MoO_3 was observed in the Mo/ZrO_2, which suggests that the interaction between Mo and ZrO_2 is weak. However, co-impregnation with Ni led to a better dispersion of MoO_3 species particles and/or less crystalline Mo species [32], which were not detectable by XRD in Ni_xMo/ZrO_2. For Ni_1Mo/ZrO_2, the obvious peak at 2θ = 44.5° was attributed to the metallic nickel phase (JCPDS 87–0712), indicating that the main active site of Ni_1Mo/ZrO_2 may be the reduced metallic nickel [33].

For Ni_1Mo/TiO_2, diffraction peaks at 27° and 36° indicated the existence of the rutile crystallites (JCPDS 88–1175), while the diffraction peaks at 25°, 48°, 54°, 55°, 69°, and 71° indicated the presence of anatase (JCPDS 84–1286), which is the majority phase in TiO_2. For $Ni_1Mo/\gamma\text{-}Al_2O_3$, the diffraction peaks at 73.2°, 45.8°, and 66.8° indicated the presence of γ-Al_2O_3 (JCPDS 010–0425). For the Ni_1Mo/Fe_2O_3, all the diffraction peaks were well matched with the standard pattern of α-Fe_2O_3 (JCPDS 33–0664). An obvious kamacite diffraction peak (44.7°,

Table 1
Textural properties of the catalysts used in hydropyrolysis experiments. (The $_x$ in Ni_xMo-doped catalysts represents the Ni/Mo molar ratio.).

Sample	S_{Bet}[a] (m^2/g)	V_{total}[b] (cm^3/g)	Mesopore size[c] (nm)	Pore Contribution (%)		Total acidity[d] (mequiv·NH_3/g)
				Micropores	Mesopores	
Ni_1Mo/Fe_2O_3	9.86	0.05	21.51	0.63	28.84	0.016
Ni_1Mo/Al_2O_3	88.08	0.19	8.23	0.50	78.44	0.357
Ni_1Mo/TiO_2	49.09	0.20	16.80	0.41	59.47	0.095
Ni_1Mo/ZrO_2	10.08	0.05	22.95	0.93	47.23	0.227
Ni_2Mo/ZrO_2	10.60	0.07	20.06	1.31	40.23	0.293
Mo/ZrO_2	5.92	0.03	21.90	1.33	23.90	0.113
ZrO_2	7.68	0.04	22.24	1.29	27.31	

[a] BET surface area is calculated from the adsorption branch of the N_2 isotherm.
[b] Total pore volumes are calculated from the N_2 adsorption at a relative pressure of 0.99.
[c] Mesopore diameter is calculated from the adsorption branch using the BJH method.
[d] Total NH_3 desorption amount in the NH_3-TPD.

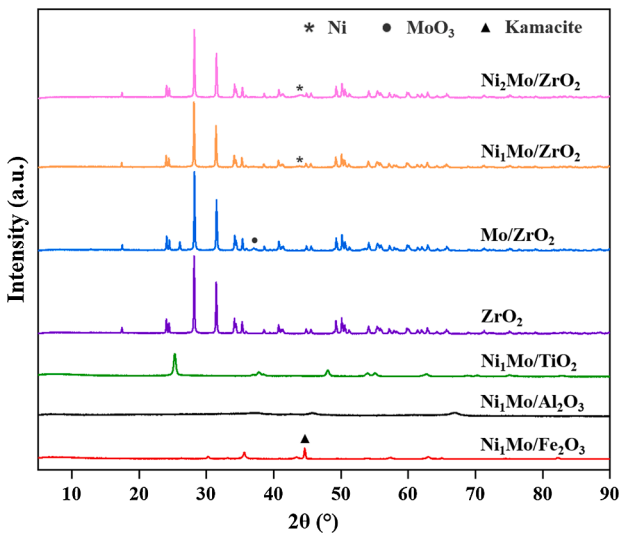

Fig. 1. X-ray diffraction patterns of the catalysts used in hydropyrolysis experiments.

PDF 37–0474) was detected on Ni_1Mo/Fe_2O_3, which shows that an alloy structure is formed between Fe and Ni. However, none of them detected obvious Ni species and Mo species, indicating that the metal species with low loading (about 5% Ni loading and 10% Mo loading) are well dispersed on these carriers [13].

The acidity of the catalysts analyzed by NH_3-TPD is shown in Fig. 2.

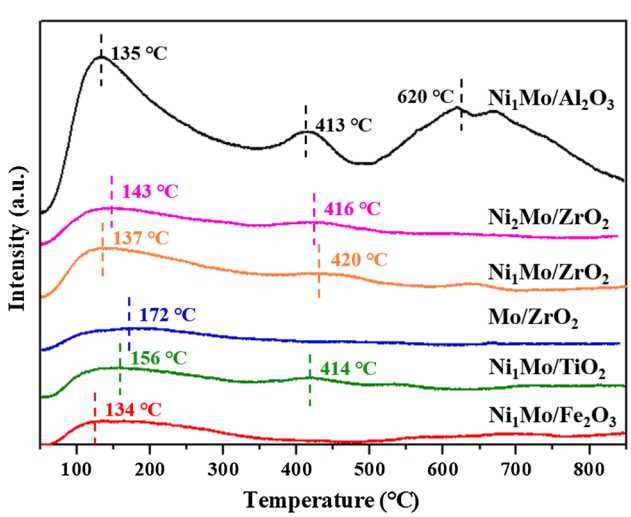

Fig. 2. NH_3-TPD profiles of the catalysts used in hydropyrolysis experiments.

The total amount of NH_3 adsorbed for catalysts is summarized in Table 1. A clear peak at about 172 °C was detected, indicating that Mo/ZrO_2 has weak acidic sites. It is worth noting that Ni_1Mo/ZrO_2 exhibited strong acid sites at about 420 °C, which indicates that the introduction of Ni can increase the strong acidity of the catalysts. With the increase of Ni loading, the total acidity of Ni_xMo/ZrO_2 increased from 0.227 mmol/g to 0.293 mmol/g, which is related to the agglomeration of Ni [34]. The sharper diffraction peak of Ni in XRD also proved the occurrence of agglomeration. Ni_1Mo/TiO_2 had moderate acidity (0.095 mmol/g), showing weak acid sites at about 156 °C and strong acid sites at about 414 °C. Ni_1Mo/Fe_2O_3 was weakly acidic, showing only weak acidic sites at 134 °C. Ni1Mo/Al_2O_3 had the strongest acidity (0.357 mmol/g), with obvious peaks at 135 °C, 413 °C, and 620 °C. Too many strong acid sites of Ni_1Mo/Al_2O_3 may lead to stronger cracking ability, which will remove the branches in the lignin structure and produce gaseous hydrocarbons [35].

The electronic interaction between Ni and Mo was investigated by XPS. The proportions of Mo and Ni in different valence states are described in Fig. 3. With the increase of Ni loading, the proportion of Ni^0 increased from 7% to 33%. The weak interaction between Ni and ZrO_2 makes NiO mainly stay on the surface of ZrO_2, so it is easier to be reduced by H_2. According to Fig. 3 **(a)**, Mo^{6+}, Mo^{5+}, Mo^{4+} existed on the surface of Mo/ZrO_2. Mo^{6+} occupied the largest proportion (48%), which makes the catalytic activity of Mo/ZrO_2 weaker. Compared to Mo/ZrO_2, the proportion of Mo^{6+} dropped significantly from 48% to 27%, and the proportion of Mo^{4+} and Mo^{3+} increased from 32% and 0% to 52% and 13%, respectively, in Ni_2Mo/ZrO_2. The loading of Ni greatly promoted the reduction of Mo species, which may be the reason for the increase in catalyst activity. This also shows that the activity of the NiMo-doped catalysts mainly depends on the intermediate oxidation species (Ni^0, Mo^{4+}, and Mo^{3+}) with a large proportion.

3.2. NiMo-doped catalysts screening

To screen a catalyst that can achieve high yield of condensable hydrocarbons and low selectivity of polyaromatics, the performance of four NiMo-doped catalysts under 1.0 MPa hydrogen was analyzed and shown in Fig. 4. The order of increasing yield of condensable hydrocarbon products was $Ni_1Mo/\gamma\text{-}Al_2O_3$ (14.03c%) < Ni_1Mo/TiO_2 (16.09c %) < Ni_1Mo/Fe_2O_3 (17.94c%) < Ni_1Mo/ZrO_2 (25.82c%). The strong acidity of $Ni_1Mo/\gamma\text{-}Al_2O_3$ as indicated by the NH_3-TPD results led to enhanced deoxygenation and cracking capability, resulting in the highest selectivity of total hydrocarbons as well as the lowest yield of condensable hydrocarbon. The moderate acidity (0.227 mmol/g) of Ni_1Mo/ZrO_2 makes it have suitable cracking and deoxidation capability under the hydropyrolysis conditions. The order of increasing selectivity of polyaromatics in condensable hydrocarbon products was $Ni_1Mo/\gamma\text{-}Al_2O_3$ (0) < Ni_1Mo/Fe_2O_3 (0.60%) < Ni_1Mo/ZrO_2 (4.37%) < Ni_1Mo/TiO_2 (7.58%). Compared to zeolite catalysts with a selectivity of about 25% [8], NiMo-doped metal oxide catalysts exhibit extremely low

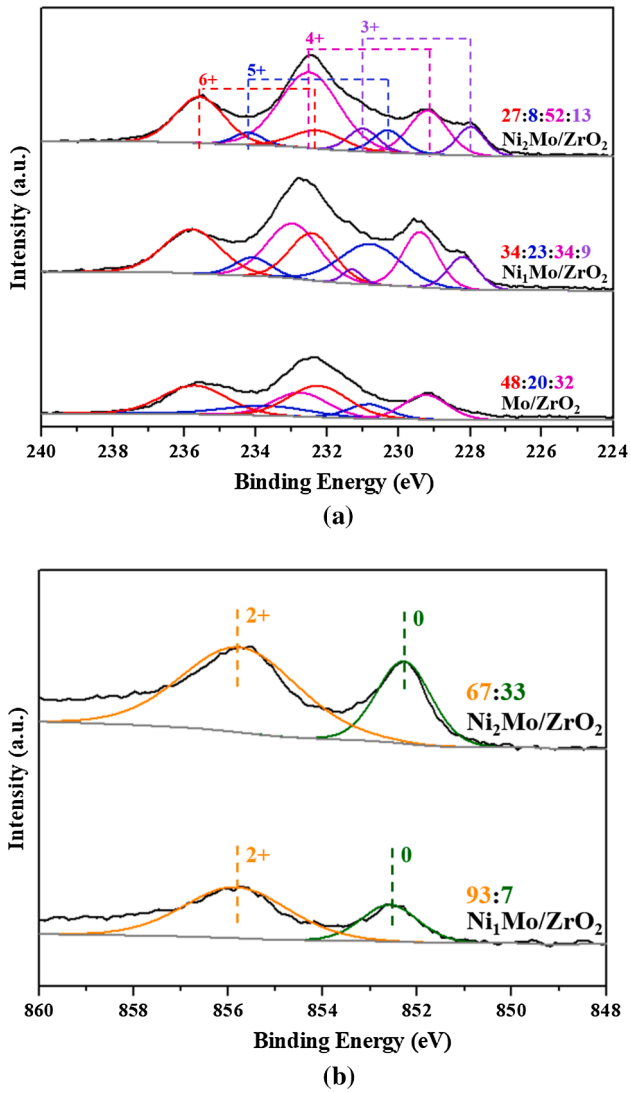

Fig. 3. XPS spectra of Ni_xMo/ZrO_2 catalysts in the ranges of (a) Ni $2p_{3/2}$ and (b) Mo 3d. The ratios displayed correspond to the proportion of oxidation states of Mo^{6+}, Mo^{5+}, Mo^{4+}, Mo^{3+}, Ni^{2+}, and Ni^0.

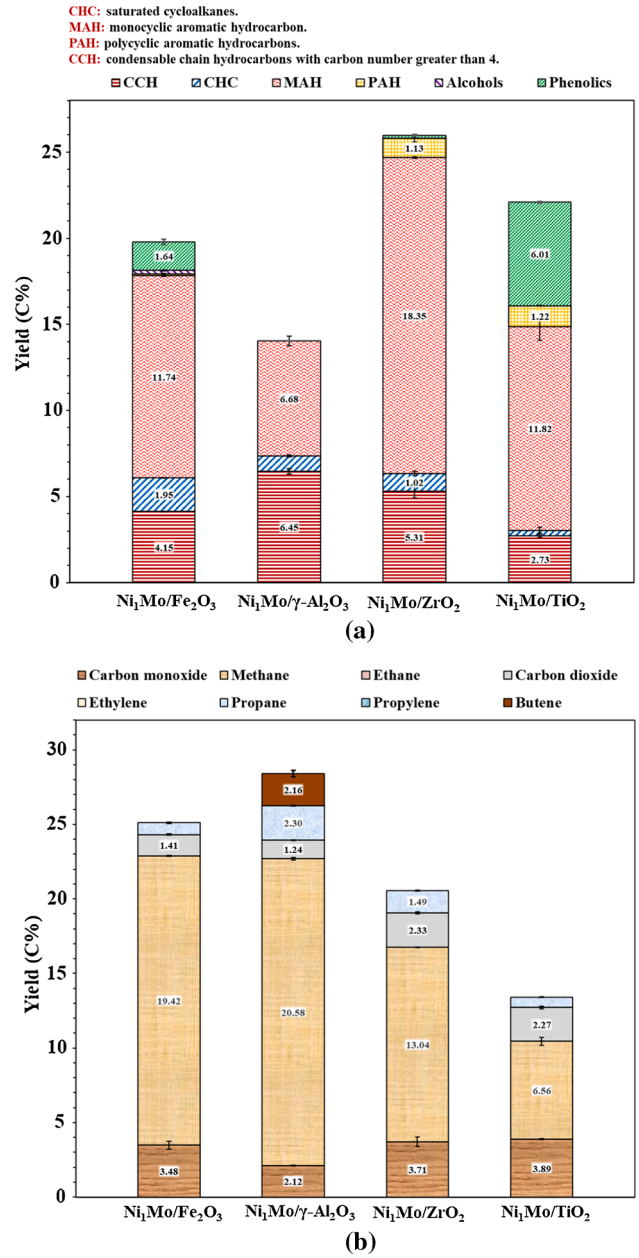

Fig. 4. Influence of carrier types of NiMo-doped catalysts on product distribution of lignin hydropyrolysis: (a) condensable vapor, (b) gaseous product. (1.0 MPa H_2, pyrolysis temperature: 500 °C, catalytic temperature: 400 °C.).

polyaromatics selectivity due to the different hydrodeoxygenation mechanisms. Aromatic hydrocarbons containing phenolic or methyl groups and five-carbon ring substances will gradually polymerize at high temperature into chemically stable polyaromatics [36]. For zeolite-based catalysts, the formation of low molecular weight aromatic hydrocarbon groups on the catalyst may undergo an aromatization reaction inside the catalyst pores to generate polyaromatics [37]. The strong cracking ability and small pore volume of NiMo-doped metal oxide catalysts in this study are not conducive to the formation of polyaromatics by aromatic hydrocarbon groups through aromatization reaction.

To reduce hydrogen consumption, the generation of gaseous hydrocarbons, especially methane, should be minimized. The increasing trend of the yield of gaseous hydrocarbons and methane yield was consistent, and the increasing order was Ni_1Mo/TiO_2 (gaseous hydrocarbons-7.26c%, methane-6.56c%) < Ni_1Mo/ZrO_2 (gaseous hydrocarbons-14.54c%, methane-13.04c%) < Ni_1Mo/Fe_2O_3 (gaseous hydrocarbons-20.22c%, methane-19.42c%) < $Ni_1Mo/\gamma\text{-}Al_2O_3$ (gaseous hydrocarbons-25.05c%, methane-20.58c%). Ni_1Mo/ZrO_2 showed a lower yield of gaseous hydrocarbons due to the moderate acidity of Ni_1Mo/ZrO_2, small pore volume and BET specific surface area, which reduces its hydrocracking capacity [38]. Based on the above quantitative data, in this study, Ni_1Mo/ZrO_2 was selected as the optimal catalyst with high condensable hydrocarbon yield, low polyaromatics yield, and low gaseous hydrocarbons yield for lignin hydropyrolysis.

3.3. Qualitative evaluation of catalytic performance

In the process of biomass catalytic hydropyrolysis, hydrocarbon products in bio-oil are mainly generated by hydrocracking reaction, hydrogenation reaction and hydrodeoxygenation reaction. The hydrocracking reaction generates gaseous hydrocarbon products by consuming condensable hydrocarbon products and hydrogen [25], which is not conducive to improving the yield of bio-oil. While the hydrogenation reaction, which saturates the benzene ring with hydrogen [39], can increase the calorific value of the liquid products. The intensity of the hydrodeoxygenation reaction, which uses hydrogen to remove the oxygen in the pyrolysis volatiles in the form of water [40], is critical to

the oxygen content of the liquid products. Therefore, in order to efficiently utilize the external hydrogen source in the production of high-quality bio-oil, it is necessary to study which reactions (hydrodeoxygenation, hydrogenation and hydrocracking) hydrogen tends to be consumed over the NiMo-doped catalysts.

HCH is introduced as a parameter to evaluate the relationship between hydrocracking reaction activity and hydrogenation reaction activity of the NiMo-doped catalysts. The increase in *HCH* indicates that hydrogen is more favored to be consumed by hydrocracking reaction than by hydrogenation reaction. As is shown in Fig. 5 **(a)**, the increasing order of *HCH* value at 1.0 MPa was Ni_1Mo/Fe_2O_3 (12.51) < Ni_1Mo/ZrO_2 (19.40) < Ni_1Mo/TiO_2 (31.71) < $Ni_1Mo/\gamma\text{-}Al_2O_3$ (41.27). Ni_1Mo/ZrO_2 showed a lower *HCH* value, which indicates that hydrogen is more likely to be consumed by hydrogenation on Ni_1Mo/ZrO_2 than on other catalysts. It can be seen from Fig. 5 **(a)** that when the hydrogen pressure increased from 1.0 MPa to 3.0 MPa, regardless of the types of catalysts, the *HCH* value decreased significantly, but was greater than 1, which indicates that the intensity of the hydrogenation reaction is gradually increasing relative to the hydrocracking reaction. This is beneficial for the efficient use of hydrogen to generate condensable hydrocarbon products. The reason for this trend is that the increasing hydrogen pressure prolonged the residence time of pyrolysis volatiles, which promotes the hydrogenation reaction of the benzene ring and secondary reactions of small molecules. However, a large number of chain hydrocarbon groups and methoxy groups on the branched-chain structure of lignin were easier to crack into gaseous hydrocarbons with a longer residence time, so the reaction was still mainly hydrocracking reaction [41].

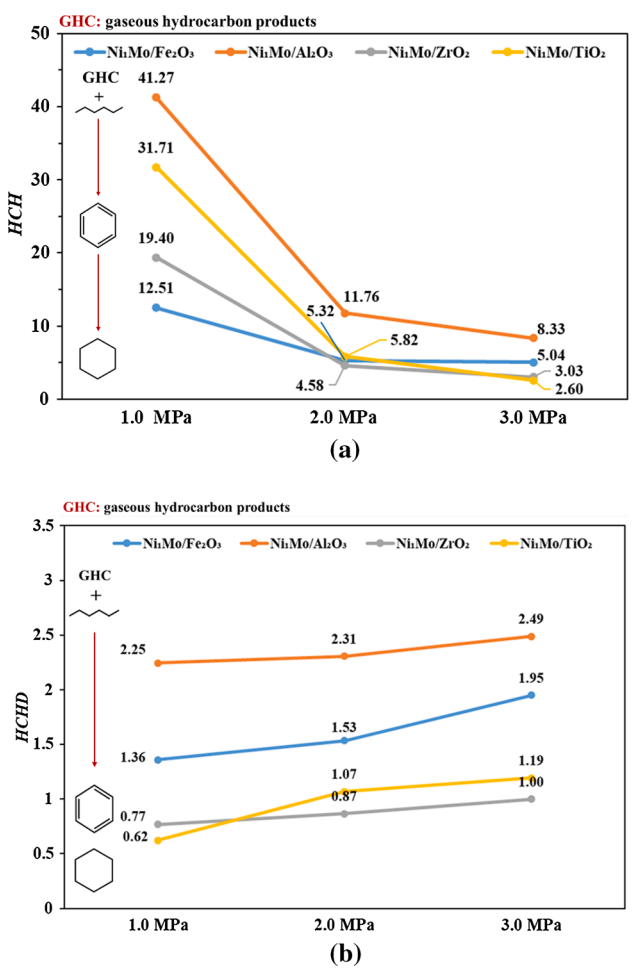

Fig. 5. Influence of hydrogen pressures and different NiMo-doped catalysts on (a) *HCH*, (b) *HCHD*. (Pyrolysis temperature: 500 °C, catalytic temperature: 400 °C.).

HCHD is used to evaluate the relationship between hydrocracking reaction activity and hydrodeoxygenation reaction activity of NiMo-doped catalysts. The increase in *HCHD* indicates that hydrogen is more likely to be consumed by hydrocracking reaction than by hydrodeoxygenation reaction. As is shown in Fig. 5 **(b)**, the increasing order of *HCHD* value at 1.0 MPa was Ni_1Mo/TiO_2 (0.62) < Ni_1Mo/ZrO_2 (0.77) < Ni_1Mo/Fe_2O_3 (1.36) < $Ni_1Mo/\gamma\text{-}Al_2O_3$ (2.25). The value of *HCHD* is close to 1 compared to the value of *HCH*, which indicates that the hydrodeoxygenation reaction activity and the hydrocracking reaction activity are comparable. This is due to Ni promotes the formation of Mo^{4+} and Mo^{3+}, which may consume the activity of Ni and enhance the activity of Mo. It is worth noting that the *HCHD* value of Ni_1Mo/ZrO_2 at 1.0 MPa H_2 was less than 1, which reveals that the hydrogen is mainly utilized by hydrodeoxygenation reaction over Ni_1Mo/ZrO_2. This helps to improve the selectivity of hydrocarbons in liquid products. Moreover, regardless of the types of NiMo-doped catalysts, as the hydrogen pressure increased, the *HCHD* value showed an upward trend. Compared with hydrodeoxygenation reaction, the increase of hydrogen pressure tends to consume hydrogen in the way of hydrocracking reaction. In order to increase the yield of condensable hydrocarbon products and increase the calorific value of liquid products, hydrogen should be utilized through hydrogenation and hydrodeoxygenation. Therefore, Ni_1Mo/ZrO_2 catalysts with low *HCH* value and *HCHD* value are considered to be the optimal catalysts for catalytic hydropyrolysis of lignin to produce hydrocarbon liquid products.

HCH and *HCHD* can help us determine in which way the hydrogen is mainly utilized over hydrodeoxygenation catalysts, which can guide the screening of catalysts for specific purposes. Meanwhile, the influence of different reaction variables (such as reaction temperature, reaction pressure) on the way the hydrogen is consumed in the catalytic pyrolysis process can also be qualitatively observed. However, it must be emphasized that *HCH* and *HCHD* can only provide qualitative guidance and cannot quantitatively assess the activity of the reaction taking place over the catalysts.

3.4. Synergistic mechanism of Ni and Mo

To study the synergistic mechanism of Ni and Mo, Ni_xMo/ZrO_2 with different Ni/Mo molar ratios were tested during lignin hydropyrolysis. The results are shown in Table 2. The yield of phenolics decreased sharply with the increase of the Ni loading, followed by Mo/ZrO_2 (12.15c%) > Ni_1Mo/ZrO_2 (0.16c%) > Ni_2Mo/ZrO_2 (0). The XPS results showed that the increase of Ni loading promotes the formation of Mo^{4+} and Mo^{3+} on the surface of the Ni_xMo/ZrO_2, which will promote the hydrodeoxygenation ability of the catalyst. The decreasing trend of phenolic products with increasing Ni loading is consistent with this inference. Leshkov et al. [42] reported Mo has the most obvious effect on the removal of phenolic methoxy groups. Thus, in order to highlight that the synergistic effect of Ni and Mo promotes the removal of the phenolic methoxy group, it is necessary to analyze the methoxy phenolics in the products. The yield of methoxy phenolics decreased with the increase of the Ni loading, followed by Mo/ZrO_2 (4.67c%) > Ni_1Mo/ZrO_2 (0.16c%) > Ni_2Mo/ZrO_2 (0). The decrease in the yield of methoxy phenolics also proved again the importance of the synergistic effect of Ni and Mo in promoting the removal of methoxy phenolics. In addition, with the introduction of Ni, CO showed a downward trend. Under the action of the Ni_2Mo/ZrO_2, the CO yield was only 3.10c% due to the interaction between Ni and Mo, which enhances the ability of Mo to deoxidize in the form of water through oxygen vacancies.

However, an excessive increase in Ni loading can also have a negative effect on the formation of condensable hydrocarbon products. With the increase of Ni loading, the total liquid yield first increased and then decreased, followed by Ni_1Mo/ZrO_2 (25.98c%) > Ni_2Mo/ZrO_2 (19.76c%) > Mo/ZrO_2 (16.83c%). When the molar ratio of Ni to Mo increased from 1 to 2, the yield of polyaromatics also decreased from 1.13c% to 0.

Table 2
Products from lignin catalytic hydropyrolysis over different catalysts. (1.0 MPa H_2, 500 °C pyrolysis temperature, 400 °C catalytic temperature.).

Yield, c%	Mo/ZrO_2	Ni_1Mo/ZrO_2	Ni_2Mo/ZrO_2
Condensable chain hydrocarbons (C greater than 4)			
n-Hexane	1.07	4.35	3.73
Heptane	0.00	0.18	0.00
Heptane, 3-methyl-	0.00	0.28	0.16
Octane	0.00	0.26	0.00
Subtotal	1.07	5.07	3.88
Saturated cycloalkanes			
Cyclohexane	0.00	0.49	0.50
Cyclohexane, methyl-	0.00	0.49	0.57
Cyclohexane, ethyl-	0.00	0.17	0.14
Cyclohexane, propyl-	0.00	0.13	0.08
Subtotal	0.00	1.27	1.29
Monocyclic aromatics			
Benzene	0.23	2.56	2.55
Toluene	0.89	5.92	5.79
Benzene, ethyl-	0.61	4.30	3.45
Benzene, propyl-	0.39	3.75	2.27
Benzene, 1-methyl-3-propyl-	0.27	1.82	0.53
Subtotal	2.38	18.35	14.59
Polyaromatics			
Naphthalene	0.00	0.46	0.00
Naphthalene, 1-methyl-	0.89	0.29	0.00
Biphenyl	0.13	0.27	0.00
1,1′-Biphenyl, 3-methyl-	0.21	0.11	0.00
Subtotal	1.23	1.13	0.00
Phenolic			
Phenol	1.37	0.00	0.00
Phenol, 2-methyl-	2.80	0.00	0.00
Phenol, 2,5-dimethyl-	2.00	0.00	0.00
Phenol, 2-ethyl-4-methyl-	0.91	0.00	0.00
2-Methyl-6-propylphenol	0.39	0.00	0.00
Benzene, methoxy-	0.00	0.16	0.00
Phenol, 2-methoxy-	0.95	0.00	0.00
Phenol, 2-methoxy-4-methyl-	1.50	0.00	0.00
3,4-Dimethoxytoluene	0.18	0.00	0.00
Phenol, 4-ethyl-2-methoxy-	1.55	0.00	0.00
Phenol, 2-methoxy-4-propyl-	0.49	0.00	0.00
Subtotal	12.15	0.16	0.00
Total liquid	16.83	25.98	19.76
Gas			
CO	5.95	3.71	3.10
CH_4	4.43	13.04	17.31
CO_2	1.72	2.33	2.50
C_3H_8	0.72	1.49	1.39
C_3H_6	0.00	0.00	1.11
Total Gas	12.82	20.57	25.42
Char (wt%)	28.34	28.45	28.94
HCH	none	3.03	18.42
HCHD	1.33	1.00	1.20
Char yield[a]	54.02	71.02	70.07

[a] According to previous research [8,43], the carbon content of char obtained from lignin hydropyrolysis at 500 °C and 1.0 MPa H_2 is assumed to be 86%.

With the increase of Ni loading, the hydrocracking reaction was enhanced, which leads to the above phenomenon. With the increase of Ni loading, the yield of gaseous hydrocarbons was followed by Ni_2Mo/ZrO_2 (19.81c%) > Ni_1Mo/ZrO_2 (14.53c%) > Mo/ZrO_2 (5.15c%). The value of *HCHD* followed by Mo/ZrO_2 (1.33) > Ni_2Mo/ZrO_2 (1.20) > Ni_1Mo/ZrO_2 (1.00). The changes in the yield of gaseous hydrocarbons and *HCHD* value indicated that too much Ni made Ni_2Mo/ZrO_2 catalyst exhibit excessive hydrocrack ability, which in turn leads to the transfer of carbon to gaseous hydrocarbons products. Therefore, when the molar ratio of Ni/Mo in NiMo-doped ZrO_2 is 1, it is most favorable for the catalytic hydropyrolysis of lignin to generate condensable hydrocarbon products.

3.5. Catalytic hydropyrolysis mechanism of lignin

Phenol, o-methoxy-, phenol, 3-methyl-, and toluene, as the main products of lignin hydropyrolysis, were used as model compounds to verify the evolution of lignin hydropyrolysis volatiles on Ni_xMo/ZrO_2 catalysts. The results are shown in Table 3.

For Mo/ZrO_2, saturated cycloalkanes and condensable chain hydrocarbons were not detected from all the three model compounds. When phenol, o-methoxy- was used as feedstock, the yield of non-methoxy phenolics was 68.14c%, while the yield of methoxy phenolics was only 3.95c%. Mo shows excellent catalytic performance for removing phenolic methoxy groups. When phenol, 3-methyl- was used as feedstock, only phenol (0.18c%) and monocyclic aromatics (5.52c%) were produced, which indicates that Mo/ZrO_2 has a limited ability to remove phenolic hydroxyl groups. Toluene almost did not convert, which confirms that Mo/ZrO_2 does not have strong hydrocracking activity. When phenol, o-methoxy- containing methoxy groups was used as feedstock, methane (6.01c%) was generated, which indicates that the methoxy groups of phenolics may be directly removed from the methyl group. Free methyl groups combined with hydrogen to form methane.

With the introduction of Ni, the yield of non-methoxy phenolics from phenol, o-methoxy- hydropyrolysis decreased from 68.14c% (Mo/ZrO_2) to 29.59c% (Ni_1Mo/ZrO_2), which infers that Ni greatly improves the ability of the catalyst to remove phenolic hydroxyl groups. The yield of methoxy phenolics was also slightly reduced from 3.95c% (Mo/ZrO_2) to 1.85c% (Ni_1Mo/ZrO_2), which shows that the interaction between Ni and Mo may promote the ability of Mo to remove methoxy groups. For Ni_1Mo/ZrO_2, when phenol, 3-methyl- was used as feedstock, the liquid products from hydropyrolysis experiments were 0.10c% phenol, 0.32c% condensable chain hydrocarbons, 3.39c% gaseous hydrocarbons, and 31.21c% monocyclic aromatics. The oxygen component was only 0.1 c% of phenol, which once again proved that Ni has a strong ability to remove phenolic hydroxyl groups. When toluene was used as feedstock, the yield of saturated cycloalkanes increased from 0 to 1.28c%, which indicates that Ni improves the ability of the catalyst to hydrogenate the benzene ring structure. The yields of condensable chain hydrocarbons and methane also increased from 0 and 0 to 0.51c% and 12.89c%, respectively, which reveals that the introduction of Ni leads to an excessively enhanced hydrocracking capacity.

The increase of Ni loading resulted in the formation of monocyclic aromatics and condensable chain hydrocarbons in the lignin model compounds hydropyrolysis. The total yield of condensable hydrocarbon products and gaseous hydrocarbons showed an increasing trend with the increase of Ni loading. For phenol, o-methoxy-, when the molar ratio of Ni and Mo increased from 1 to 2, the yield of condensable hydrocarbon products and gaseous hydrocarbons increased from 29.83c% and 7.53c % to 33.50c% and 10.37c%, respectively. The results showed that the increased loading of Ni greatly improves the hydrocracking ability of the catalyst.

To show the catalysis of Ni_1Mo/ZrO_2 more clearly, the evolution path of volatiles from lignin hydropyrolysis over the Ni_1Mo/ZrO_2 catalyst is depicted in Fig. 6. The methoxy groups in the phenolic monomers obtained from lignin hydropyrolysis are preferentially removed by Mo to generate non-methoxy phenolics. Non-methoxy phenolics first are removed phenolic hydroxyl groups to generate aromatic hydrocarbons under Ni catalysis, and then aromatic hydrocarbons generate saturated cycloalkanes through hydrogenation reaction. Saturated cycloalkanes are further broken to form condensable chain hydrocarbons.

4. Conclusion

The catalytic hydropyrolysis experiments of lignin and its model compounds were carried out over NiMo-doped catalysts with different carriers and Ni/Mo molar ratios. The catalyst with Ni/Mi ratio of 1 with ZrO_2 as carrier (Ni_1Mo/ZrO_2) exhibits excellent catalytic activity in lignin catalytic hydropyrolysis at 1.0 MPa H_2 and 400 °C catalytic

Table 3
Products from catalytic hydropyrolysis of phenol, o-methoxy-, phenol, 3-methyl-, and toluene. (1.0 MPa H_2, 500 °C pyrolysis temperature, 400 °C catalytic temperature.).

Compound, c%	**Mo/ZrO_2**			**Ni_1Mo/ZrO_2**			**Ni_2Mo/ZrO_2**		
	phenol, o-methoxy-	phenol, 3-methyl-	toluene	phenol, o-methoxy-	phenol, 3-methyl-	toluene	phenol, o-methoxy-	phenol, 3-methyl-	toluene
Condensable chain hydrocarbons (C greater than 4)									
Pentane	0.00	0.00	0.00	1.16	0.11	0.15	1.79	0.13	0.17
1-Pentene	0.00	0.00	0.00	0.00	0.03	0.18	0.46	0.35	0.20
n-Hexane	0.00	0.00	0.00	0.27	0.00	0.18	0.06	0.11	0.25
3-Hexene, (Z)-	0.00	0.00	0.00	0.10	0.17	0.00	0.36	0.00	0.00
Subtotal	0.00	0.00	0.00	1.54	0.32	0.51	2.68	0.59	0.61
Saturated cycloalkanes									
Cyclohexane	0.00	0.00	0.00	4.46	0.21	0.31	5.00	0.40	0.31
Cyclohexane, methyl-	0.00	0.00	0.00	0.41	3.18	0.97	0.72	6.29	0.95
Subtotal	0.00	0.00	0.00	4.86	3.39	1.28	5.71	6.69	1.26
Monocyclic aromatics									
Benzene	0.65	0.00	2.19	17.31	0.94	3.56	18.19	1.55	4.85
Toluene	1.17	5.52	97.07	5.48	30.12	82.89	5.76	44.83	74.16
Benzene, 1,4-dimethyl-	0.00	0.00	0.00	0.20	0.16	0.24	0.61	0.24	0.29
Benzene, ethyl-	0.00	0.00	0.00	0.09	0.00	0.05	0.15	0.00	0.06
Subtotal[a]	1.82	5.52	2.19	23.09	31.21	3.85	24.70	46.62	5.20
Polyaromatics									
Bibenzyl	0.00	0.00	0.00	0.00	0.00	0.00	0.18	0.00	0.00
Diphenylmethane	0.00	0.00	0.00	0.34	0.00	0.00	0.22	0.00	0.00
Subtotal	0.00	0.00	0.00	0.34	0.00	0.00	0.40	0.00	0.00
Phenolics									
Benzene, methoxy-	3.34	0.00	0.00	1.67	0.00	0.00	1.56	0.00	0.00
Phenol	32.28	0.18	0.00	16.08	0.10	0.00	15.94	0.11	0.00
Phenol, o-methoxy-	23.89	0.00	0.00	8.36	0.00	0.00	7.82	0.00	0.00
Phenol, 3-methyl-	29.96	68.78	0.00	12.17	34.10	0.00	11.78	11.75	0.00
Benzene, 1-methoxy-3-methyl-	0.31	0.00	0.00	0.00	0.00	0.00	0.00	0.00	0.00
Benzene, 1,2-dimethoxy-	0.31	0.00	0.00	0.18	0.00	0.00	0.14	0.00	0.00
Phenol, 2,3-dimethyl-	2.38	0.00	0.00	1.33	0.00	0.00	1.46	0.00	0.00
Catechol	2.52	0.00	0.00	0.00	0.00	0.00	0.00	0.00	0.00
Subtotal[a]	71.09	0.18	0.00	31.44	0.10	0.00	30.88	0.11	0.00
Total liquid yield[a]	72.92	5.70	2.19	61.27	69.12	5.64	64.38	54.01	7.07
Gas									
CO	0.36	0.00	0.00	0.63	0.66	0.00	0.57	1.34	0.00
CH_4	6.01	0.00	0.00	6.62	2.12	12.89	8.71	2.25	16.37
C_2H_4	0.00	0.00	0.00	0.18	0.07	1.17	0.36	0.11	1.42
C_3H_6	0.00	0.00	0.00	0.23	0.50	0.99	0.42	0.49	1.21
C_4H_8	0.00	0.00	0.00	0.50	0.33	0.38	0.88	0.34	0.73
Total gas yield	6.37	0.00	0.00	8.15	3.68	15.43	10.94	4.52	19.73
Total condensable hydrocarbon	1.82	5.52	2.19	29.83	34.92	5.64	33.50	53.90	7.07
Non-methoxy phenolics[a]	67.14	0.18	0.00	29.59	0.10	0.00	29.18	0.11	0.00
Methoxy-phenolics[a]	3.95	0.00	0.00	1.85	0.00	0.00	1.70	0.00	0.00
Carbon balance	103.17	74.48	99.26	77.78	72.80	103.96	83.13	70.28	100.96
Conversion%	76.11	31.22	2.93	91.64	65.90	100.00	92.18	88.25	99.94

[a] Did not include the remaining amount of feedstock.

temperature. Over the Ni_1Mo/ZrO_2 catalyst, the highest yield of condensable hydrocarbons was 25.82c%. High yield of condensable chain hydrocarbons (5.31c%) and monocyclic aromatics (18.35c%) were obtained. Meanwhile, the formation of methane was suppressed due to the optimal NiMo molar ratio and carrier, which leads to moderate hydrocracking capacity. The XPS results indicate that the activity of Ni_xMo/ZrO_2 mainly depends on Ni^0, Mo^{4+}, and Mo^{3+}. The synergistic effect of Ni and Mo promotes the removal of the phenolic methoxy group. When the molar ratio of Ni/Mo in NiMo-doped ZrO_2 is 1, it is most favorable for the catalytic hydropyrolysis of lignin to generate condensable hydrocarbon products.

To qualitatively evaluate the catalytic performance of NiMo-doped catalysts, two coefficients of *HCH* and *HCHD* were introduced. Compared to other NiMo-doped catalysts, the lower *HCH* value (19.40) and *HCHD* value (0.77) of Ni_1Mo/ZrO_2 at 1.0 MPa H_2 infers that hydrogen was efficiently utilized through hydrogenation and hydrodeoxygenation over Ni_1Mo/ZrO_2. The increase of hydrogen pressure makes the *HCH* value decrease and the *HCHD* value increase, which indicates that the increase of hydrogen pressure tends to utilize hydrogen through hydrogenation reaction and hydrocracking.

The results of the lignin model compound hydropyrolysis show that Mo promotes the cleavage of phenolic methoxy groups. Ni promotes the cleavage of phenolic hydroxyl groups and the hydrogenation reaction of benzene ring. The evolution process of lignin hydropyrolysis volatiles under the effect of Ni_1Mo/ZrO_2 was clarified. During lignin catalytic hydropyrolysis, the methoxy phenolics are preferentially removed methoxy groups by Mo, while the phenolics of non-methoxy group are catalyzed by Ni to remove the phenolic hydroxyl groups to generate aromatics. Under the catalysis of Ni, aromatics generate saturated cycloalkanes through hydrogenation reaction, which will be further broken to form condensable chain hydrocarbons.

CRediT authorship contribution statement

Tan Li: Experimental Program Design, Experimental Operation, Investigation, Data Curation, Data Analysis, Writing - Original Draft, Writing - Review & Editing, Visualization. **Jing Su:** Experimental Operation, Data Analysis, Review & Editing. **Huiyuan Wang:** Data Analysis, Review & Editing. **Cong Wang:** Experimental Operation, Review & Editing. **Wen Xie:** Investigation, Review & Editing. **Kaige**

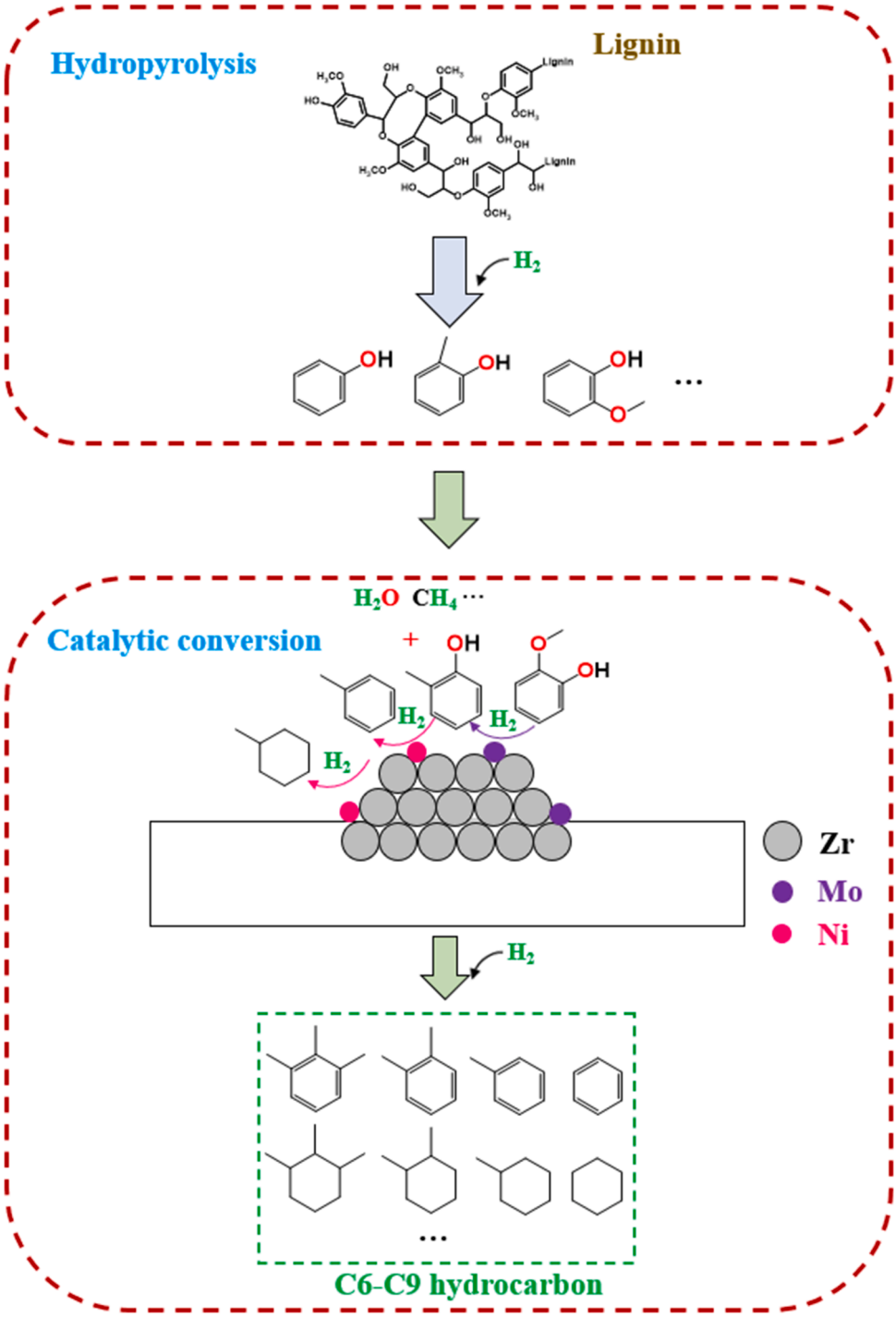

Fig. 6. Formation pathways of hydrocarbon products from lignin hydropyrolysis over the catalysis of Ni_xMo/ZrO_2.

Wang: Resources, Writing - Review & Editing, Supervision, Project Administration, Funding Acquisition.

Declaration of Competing Interest

The authors declare that they have no known competing financial interests or personal relationships that could have appeared to influence the work reported in this paper.

Acknowledgments

The authors would like to acknowledge financial support from the National Natural Science Foundation of China (Grant No.: 51906215) and the Fundamental Research Funds for the Central Universities.

Appendix A. Supplementary material

Supplementary data to this article can be found online at https://doi.org/10.1016/j.apenergy.2022.119115.

References

[1] Chen J, Liu C, Wu S, Liang J, Lei M. Enhancing the quality of bio-oil from catalytic pyrolysis of kraft black liquor lignin. RSC Adv 2016;6(109):107970–6.

[2] Andrade MC, Gorgulho Silva CO, de Souza Moreira LR, Ferreira Filho EX. Crop residues: applications of lignocellulosic biomass in the context of a biorefinery. Frontiers. Energy 2021.

[3] Zhong D, Zeng K, Li J, Qiu Yi, Flamant G, Nzihou A, et al. Characteristics and evolution of heavy components in bio-oil from the pyrolysis of cellulose, hemicellulose and lignin. Renew Sustain Energy Rev 2022;157:111989. https://doi.org/10.1016/j.rser.2021.111989.

[4] Liu C, Hu J, Zhang H, Xiao R. Thermal conversion of lignin to phenols: Relevance between chemical structure and pyrolysis behaviors. Fuel 2016;182:864–70.

[5] Pandey MP, Kim CS. Lignin Depolymerization and Conversion: A Review of Thermochemical Methods. Chem Eng Technol 2011;34(1):29–41.

[6] Li W, Zhou S, Xue Y, Lee Y-J, Smith R, Bai X. Understanding Low-Pressure Hydropyrolysis of Lignin Using Deuterated Sodium Formate. Acs Sustain Chem Eng 2017;5(10):8939–50.

[7] Stanton AR, Iisa K, Mukarakate C, Nimlos MR. Role of Biopolymers in the Deactivation of ZSM-5 during Catalytic Fast Pyrolysis of Biomass. Acs Sustain Chem Eng 2018;6(8):10030–8.

[8] Xue Y, Sharma A, Huo J, Qu W, Bai X. Low-pressure two-stage catalytic hydropyrolysis of lignin and lignin-derived phenolic monomers using zeolite-based bifunctional catalysts. J Anal Appl Pyrol 2020;146:104779. https://doi.org/10.1016/j.jaap.2020.104779.

[9] Zhang X, Tang J, Zhang Qi, Liu Q, Li Y, Chen L, et al. Hydrodeoxygenation of lignin-derived phenolic compounds into aromatic hydrocarbons under low hydrogen pressure using molybdenum oxide as catalyst. Catal Today 2019;319:41–7.

[10] Prasomsri T, Shetty M, Murugappan K, Román-Leshkov Y. Insights into the catalytic activity and surface modification of MoO3 during the hydrodeoxygenation of lignin-derived model compounds into aromatic hydrocarbons under low hydrogen pressures. Energy Environ Sci 2014;7(8):2660–9.

[11] Liu Y, Leahy JJ, Grams J, Kwapinski W. Hydro-Pyrolysis and Catalytic Upgrading of Biomass and Its Hydroxy Residue Fast Pyrolysis Vapors. Energies 2019;12(18):3474. https://doi.org/10.3390/en12183474.

[12] Shi J, Sun L, Yan H, Wang J. Catalytic Hydrotreatment of Pine Sawdust Hydropyrolysis Vapor over Ni, Mo-Impregnated HZSM-5 for Optimal Production of Gasoline Components. Energ. Fuel 2022;36(2):932–44.

[13] Yu P, Fang M, Ma S, Cen J, Luo Z. Quantitative evaluation of coupling effects of pore structures and metal loadings on catalytic hydrogenation of tar model reactants over sulfided NiMo/γ-Al2O3 catalysts: Role of segmented catalytic active phase volumes. Fuel Process Technol 2021;224:107008. https://doi.org/10.1016/j.fuproc.2021.107008.

[14] Dayton DC, Hlebak J, Carpenter JR, Wang K, Mante OD, Peters JE. Biomass Hydropyrolysis in a Fluidized Bed Reactor. Energ Fuel 2016;30(6):4879–87.

[15] Stummann MZ, Hansen AB, Hansen LP, Davidsen B, Rasmussen SB, Wiwel P, et al. Catalytic Hydropyrolysis of Biomass Using Molybdenum Sulfide Based Catalyst. Effect of Promoters Energ Fuel 2019;33(2):1302–13.

[16] Guo S, Wei X, Che D, Liu H, Sun B. Experimental study on influence of operating parameters on tar components from corn straw gasification in fluidized bed. Frontiers in Energy 2021;15(2):374–83.

[17] Mei D, Karim AM, Wang Y. Density Functional Theory Study of Acetaldehyde Hydrodeoxygenation on MoO3. The Journal of Physical Chemistry C 2011;115(16):8155–64.

[18] Wang C, Jia Q, Nakagawa N, Kato K. Conversion of plant-biomass to BTX and synthetic fuels by catalytic pyrolysis. Journal of Chemical Industry and Engineering (China) 2004;55:1341–7.

[19] Yu L, Farinmade A, Ajumobi O, John VT, Valla JA. One-Step Hydropyrolysis and Hydrotreating Tandem Reactions of Miscanthus × giganteus Using Ni Impregnated ZSM-5/MCM-41 Composites. Energ Fuel 2021;35(24):20117–30.

[20] Chandler DS, Seufitelli GVS, Resende FLP. Catalytic Route for the Production of Alkanes from Hydropyrolysis of Biomass. Energ Fuel 2020;34(10):12573–85.

[21] Resende KA, Braga AH, Noronha FB, Hori CE. Hydrodeoxygenation of phenol over Ni/Ce1-xNbxO2 catalysts. Appl Catal B-Environ 2019;245:100–13.

[22] Yang Y, Ochoa-Hernández C, de la Peña O'Shea VA, Pizarro P, Coronado JM, Serrano DP. Effect of metal-support interaction on the selective hydrodeoxygenation of anisole to aromatics over Ni-based catalysts. Appl Catal B-Environ 2014;145:91–100.

[23] El Hage R, Brosse N, Chrusciel L, Sanchez C, Sannigrahi P, Ragauskas A. Characterization of milled wood lignin and ethanol organosolv lignin from miscanthus. Polym Degrad Stab 2009;94(10):1632–8.

[24] Huang F, Singh PM, Ragauskas AJ. Characterization of milled wood lignin (MWL) in Loblolly pine stem wood, residue, and bark. J Agric Food Chem 2011;59(24):12910–6.

[25] He Y, Zhao Y, Chai M, Zhou Z, Sarker M, Li C, et al. Comparative study of fast pyrolysis, hydropyrolysis and catalytic hydropyrolysis of poplar sawdust and rice husk in a modified Py-GC/MS microreactor system: Insights into product distribution, quantum description and reaction mechanism. Renew Sust Energ Rev 2020;119:109604. https://doi.org/10.1016/j.rser.2019.109604.

[26] Anderson AD, Lanci MP, Buchanan JS, Dumesic JA, Huber GW. The Hydrodeoxygenation of Glycerol over NiMoSx: Catalyst Stability and Activity at Hydropyrolysis Conditions. ChemCatChem 2021;13(1):425–37.

[27] Yoon JS, Lee Y, Ryu J, Kim Y-A, Park ED, Choi J-W, et al. Production of high carbon number hydrocarbon fuels from a lignin-derived alpha-O-4 phenolic dimer, benzyl phenyl ether, via isomerization of ether to alcohols on high-surface-area silica-alumina aerogel catalysts. Appl Catal B-Environ 2013;142:668–76.

[28] Joffres B, Lorentz C, Vidalie M, Laurenti D, Quoineaud A-A, Charon N, et al. Catalytic hydroconversion of a wheat straw soda lignin: Characterization of the products and the lignin residue. Appl Catal B-Environ 2014;145:167–76.

[29] Sirous-Rezaei P, Creaser D, Olsson L. Reductive liquefaction of lignin to monocyclic hydrocarbons: ReS2/Al2O3 as efficient char inhibitor and hydrodeoxygenation catalyst. Appl Catal B-Environ 2021;297:120449. https://doi.org/10.1016/j.apcatb.2021.120449.

[30] Teixeira CM, Fréty R, Barbosa CBM, Santos MR, Bruce ED, Pacheco JGA. Mo influence on the kinetics of jatropha oil cracking over Mo/HZSM-5 catalysts. Catal Today 2017;279:202–8.

[31] Calafat Á, Sánchez N. Production of carbon nanotubes through combination of catalyst reduction and methane decomposition over Fe–Ni/ZrO2 catalysts prepared by the citrate method. Appl Catal A 2016;528:14–23.

[32] Yang F, Libretto NJ, Komarneni MR, Zhou W, Miller JT, Zhu X, et al. Enhancement of m-Cresol Hydrodeoxygenation Selectivity on Ni Catalysts by Surface Decoration of MoOx Species. Acs Catal 2019;9(9):7791–800.

[33] Pan L, He Y, Niu M, Dan Y, Li W. Selective hydrodeoxygenation of p-cresol as a model for coal tar distillate on Ni-M/SiO2 (M = Ce Co, Sn, Fe) bimetallic catalysts. RSC Adv 2019;9(37):21175–85.

[34] Zheng Y, Zhao N, Chen J. Enhanced direct deoxygenation of anisole to benzene on SiO2-supported NiGa alloy and intermetallic compound. Appl Catal B-Environ 2019;250:280–91.

[35] Li Y, Ma L, Liu H, He D. Influence of HZSM5 on the activity of Ru Catalysts and product selectivity during the hydrogenolysis of glycerol. Applied Catalysis a-General 2014;469:45–51.

[36] Baldwin RM, Magrini-Bair KA, Nimlos MR, Pepiot P, Donohoe BS, Hensley JE, et al. Current research on thermochemical conversion of biomass at the National Renewable Energy Laboratory. Appl Catal B-Environ 2012;115-116:320–9.

[37] Williams PT, Horne PA. THE INFLUENCE OF CATALYST TYPE ON THE COMPOSITION OF UPGRADED BIOMASS PYROLYSIS OILS. J Anal Appl Pyrol 1995;31:39–61.

[38] Castaño P, Gutiérrez A, Villanueva I, Pawelec B, Bilbao J, Arandes JM. Effect of the support acidity on the aromatic ring-opening of pyrolysis gasoline over Pt/HZSM-5 catalysts. Catal Today 2009;143(1-2):115–9.

[39] Yan P, Mensah J, Adesina A, Kennedy E, Stockenhuber M. Highly-dispersed Ni on BEA catalyst prepared by ion-exchange-deposition-precipitation for improved hydrodeoxygenation activity. Appl Catal B-Environ 2020;267:118690. https://doi.org/10.1016/j.apcatb.2020.118690.

[40] Mochizuki T, Chen S-Y, Toba M, Yoshimura Y. Deoxygenation of guaiacol and woody tar over reduced catalysts. Appl Catal B-Environ 2014;146:237–43.

[41] Chen Q, Cai C, Zhang X, Zhang Qi, Chen L, Li Y, et al. Amorphous FeNi-ZrO2-Catalyzed Hydrodeoxygenation of Lignin-Derived Phenolic Compounds to Naphthenic Fuel. Acs Sustain Chem Eng 2020;8(25):9335–45.

[42] Shetty M, Murugappan K, Prasomsri T, Green WH, Román-Leshkov Y. Reactivity and stability investigation of supported molybdenum oxide catalysts for the hydrodeoxygenation (HDO) of m-cresol. J Catal 2015;331:86–97.

[43] Ma Z, Yang Y, Wu Y, Xu J, Peng H, Liu X, et al. In-depth comparison of the physicochemical characteristics of bio-char derived from biomass pseudo components: Hemicellulose, cellulose, and lignin. J Anal Appl Pyrol 2019;140:195–204.